Evaluation of Experimental Liver Tumors Using Fluorine-18-2-Fluoro-2-Deoxy-D-Glucose PET

Natsuo Oya, Yasushi Nagata, Takashi Ishigaki, Mitsuyuki Abe, Nagara Tamaki, Yasuhiro Magata and Junji Konishi

Departments of Radiology and Nuclear Medicine, Faculty of Medicine, Kyoto University, Kyoto, Japan

Japanese white rabbits transplanted with VX2 liver tumors are considered to be a suitable experimental model for the evaluation of therapeutic modalities. However, there has been no adequate method of assessing the changes of tumor metabolism during treatment. In the present study, 15 rabbits with VX2 liver tumors were examined by PET using ^{18}F-2-fluoro-2-deoxy-D-glucose (^{18}F-FDG). After an intravenous injection of ^{18}F-FDG, serial arterial blood sampling was performed. One hour after tracer injection, small pieces of normal liver tissue and tumor tissue were excised to determine radioactivity. Dynamic PET images were obtained in 11 of the tumor-bearing rabbits, and tumor enzyme activities were determined in six rabbits. Fluorine-18-FDG uptake by the VX2 liver tumors was 3.5 ± 0.9 times higher than that by the normal liver tissue; so good contrast between tumor and normal liver tissue was achieved on PET scans. The enzyme activity study showed that VX2 tumors had increased levels of hexokinase and pyruvate kinase activity, suggesting an increase of glycolysis. We conclude that transplanted VX2 liver tumors could be appropriately evaluated by ^{18}F-FDG PET.

J Nucl Med 1993; 34:2124–2129

Malignant tumor cells have intense glycolytic activity and consequently an increased level of exogenous glucose utilization (*1–3*). This increase in glucose metabolism can be assessed quantitatively using ^{18}F-2-fluoro-2-deoxy-D-glucose (^{18}F-FDG), a fluorinated glucose analog, and PET. Fluorine-18-FDG and glucose are competitive substrates for transportation from plasma to the tissues or for phosphorylation by hexokinase, but the former is trapped intracellularly in a phosphorylated form because of its low rate of subsequent metabolization, low membrane permeability, and low dephosphorylation rate (*4,5*), while the latter enters the glycolytic pathway.

Increased ^{18}F-FDG uptake has been reported in human brain tumors (*6,7*) and in tumors of other organ systems (*8–19*), including liver tumors (*16–19*). These studies have demonstrated the utility of ^{18}F-FDG PET for tumor detection as well as for making a differential diagnosis and evaluating treatment. Data on the uptake of ^{18}F-FDG or other tracers which support the clinical utility of these agents in experimental tumor models have also been reported (*20–25*). However, experimental liver tumors have not previously been evaluated by ^{18}F-FDG PET. Compared with other organs, the liver has some special features with regard to ^{18}F-FDG PET studies. Because the surrounding normal liver tissue has a high glucose-6-phosphatase activity with the consequent rapid dephosphorylation of ^{18}F-FDG-6-phosphate, the lower background radioactivity provides a clearer image, as has been clinically demonstrated in several studies.

In the present study, we evaluated VX2 liver tumors using ^{18}F-FDG PET to compare the uptake profile of this liver tumor model with that previously reported for human liver tumors and to determine the applicability of this model to the investigation of human liver tumors. We also assessed enzyme activity in this liver tumor model to approach the mechanism underlying the increased ^{18}F-FDG uptake.

MATERIALS AND METHODS

Animals and Tumors

Fifteen male Japanese white rabbits (weighing 2–3 kg) bearing VX2 tumors in the liver were used in this study.

Tumor tissue samples were stored frozen as small blocks about 1 mm in diameter and contained approximately 1×10^6 VX2 sarcoma cells. Rabbits were anesthetized with sodium pentobarbital, a midline abdominal incision was made and several blocks of VX2 tumor tissue were transplanted directly into the liver. CT scanning was performed 3 wk after transplantation and the rabbits with liver tumors over 2 cm in diameter were used in the following experiments. Figure 1 shows the CT appearance of a VX2 liver tumor.

Radiopharmaceutical Agent

Fluorine-18 was produced by the ^{20}Ne(d, α)^{18}F nuclear reaction using an ultracompact cyclotron (Sumitomo, CYPRIS-model-325). Fluorine-18-FDG was then synthesized by the acetylhypofluorite method of Shiue et al. (*26*) with slight modification. The specific activity of ^{18}F-FDG was 143–204 MBq/mg, and the radiochemical purity was over 95% assessed by HPLC (Shimadzu,

Received Nov. 24, 1992; revision accepted Jul. 25, 1993.

For correspondence and reprints contact: Natsuo Oya, MD, Department of Radiology, Kyoto University Hospital, 54 Kawahara-cho, Shogoin, Sakyo-ku, Kyoto 606, Japan.

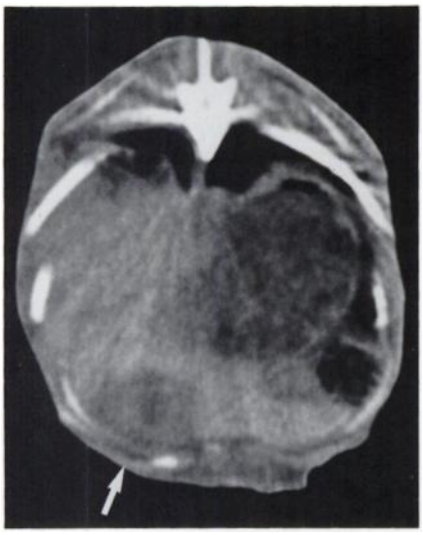

FIGURE 1. CT scan of a VX2 liver tumor (arrow).

LC-10AS; column, Carbohydrate, Waters; eluent, $CH_3CN:H_2O$ = 85:15).

Fluorine-18-FDG Injection and Arterial Blood Sampling

Tumor-bearing rabbits were anesthetized with sodium pentobarbital (25 mg/kg body weight) after 4 hr of fasting and then received an intravenous injection of 8–25 MBq/kg body weight of ^{18}F-FDG. Fluorine-18-FDG was injected via an auricular vein over a 30-sec period and the time of starting injection was defined as time 0.

Arterial blood sampling was performed in 15 rabbits (rabbits 1–15). Two milliliters of blood were sampled from a catheter introduced into the femoral artery at 15, 30, 45, 60, 75 and 90 sec, as well as 2, 3, 5, 8, 15, 25, 40 and 60 min after ^{18}F-FDG injection. These blood samples were centrifuged for 5 min at 3000 rpm to collect plasma; the plasma radioactivity level was measured with an automated NaI well scintillation counter (Packard Auto-Gamma 500, Packard Instrument, Chicago, IL).

Tissue Excision

Tissue specimens were obtained from 11 rabbits (rabbits 1–11). Immediately after the last arterial blood sample was obtained (60 min after ^{18}F-FDG injection), each rabbit was killed with a lethal dose of pentobarbital, and a number of small pieces of tumor tissue and normal liver were excised for the counting of radioactivity.

Dynamic PET Imaging

PET images were obtained with an animal PET camera (SHR-2000; Hamamatsu Photonics, Hamakita, Japan). The transaxial and axial resolution of the system was respectively 3.0 mm and 4.8 mm (FWHM) at the center of the field of view. The slice aperture was 8 mm, and the averaged direct slice sensitivity and cross slice sensitivity were respectively 2.3 kcps/μCi/ml and 3.8 kcps/μCi/ml. Total system sensitivity was 20.7 kcps/μCi/ml including the scatter component (*27*).

Fluorine-18-FDG PET scanning was performed on 11 rabbits (rabbits 5–15). Each anesthetized rabbit was fixed in the gantry of the camera and a transmission scan was obtained for 15 min with a ^{68}Ge ring. Sequential 2-min or 3-min scans then were obtained over the 60-min period following ^{18}F-FDG injection.

Enzyme Activity Assays

The activity of key carbohydrate-metabolizing enzymes was determined in six tumor-bearing rabbits. Normal liver tissue and tumor tissue specimens were frozen immediately after excision. The following enzymes were assayed: hexokinase (HK), glucokinase (GK), phosphofructokinase (PFK), pyruvate kinase (PK), glucose-6-phosphate dehydrogenase (G6PDH), fructose-1,6-diphosphatase (FDPase) and glucose-6-phosphatase (G6Pase). Tissue homogenates were used to determine G6Pase activity, and the homogenates were centrifuged for 30 min at 15000 rpm to obtain supernatants for determining the other enzyme activities (*28–30*).

RESULTS

Plasma ^{18}F Levels

As shown in Figure 2, the peak level of ^{18}F radioactivity in arterial plasma ($C_P(t)$, open squares) occurred in the first 3 min, after which ^{18}F levels decreased consistently. Plasma glucose levels ranged from 111 to 241 g/dl, which would not influence significantly the clearance of ^{18}F. Arterial input (AI) was calculated as follows:

$$AI = \int_0^{60} C_P(t)\, dt.$$

AI varied with the dose of ^{18}F-FDG and ranged from 6.1×10^5 to 4.2×10^6(Bq/ml) $\times$ min.

Fluorine-18 Levels in Liver and Tumor Tissue

The radioactivity in the tumor specimens excised 60 min after ^{18}F-FDG injection (C_t, small closed circles) was markedly higher than that in normal liver tissue (C_l, small open circles) (Fig. 2A–B). The ratio of tumor uptake-to-normal liver tissue uptake (C_t/C_l, tumor-to-normal liver ratio) was 3.5 ± 0.9 (mean ± s.d.) in 11 rabbits. The tumor uptake to AI (C_t-to-AI) ratio was 0.044 ± 0.009 min^{-1} (mean ± s.d.), while the normal liver uptake-to-AI (C_l-to-AI) ratio was 0.013 ± 0.003 min^{-1} (mean ± s.d.).

PET Imaging

Dynamic PET images were obtained from 11 rabbits. In these images, the tumors could be clearly distinguished from the surrounding normal liver tissue. Figure 3 shows the PET images obtained in the last 3-min scan. Regions of interest were fixed for the tumor and normal liver, and serial changes of tumor radioactivity ($C_T(t)$, closed circles) and normal liver radioactivity ($C_L(t)$, open circles) were plotted versus time (Fig. 2B–C). Tumor ^{18}F concentration increased continuously, whereas that of normal liver decreased almost in parallel to that of arterial plasma. In seven rabbits (rabbits 5–11), the ^{18}F-FDG concentration of tumor tissue and normal liver tissue was measured both in vitro by excised tissue counting and in vivo by PET imaging. As shown in Table 1 and Figure 2B, the PET values ($C_T(60)$ and $C_L(60)$) were close to the respective in vitro values (C_t and C_l) at 60 min after ^{18}F-FDG injection.

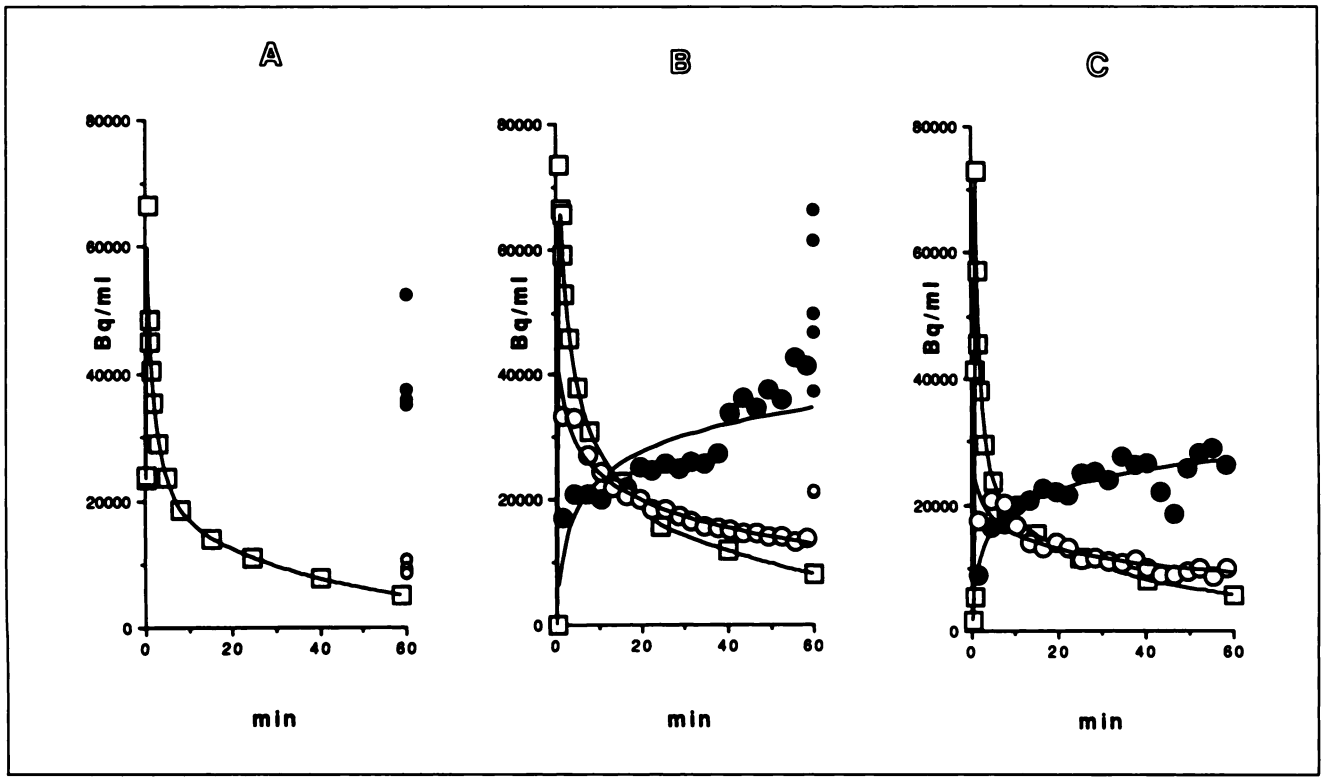

FIGURE 2. Time course of ^{18}F-FDG radioactivity in arterial blood plasma, tumor tissue and normal liver tissue. (A) Rabbit 4; (B) rabbit 8; (C) rabbit 15. Fluorine-18 radioactivity in: □, arterial plasma ($C_P(t)$); ●, in tumor ($C_T(t)$); ○, in normal liver ($C_L(t)$); •, in excised tumor (C_t); and ○, in excised normal liver (C_l).

Enzyme Activities

The activities of seven key carbohydrate-metabolizing enzymes in tumor tissue and normal liver tissue are presented in Table 2. Compared with normal liver tissue, transplanted VX2 liver tumor tissue showed an increase of HK and PK activity as well as a decrease of G6Pase and FDPase activity. GK, PFK and G6PDH did not show any significant differences in activity between normal liver tissue and tumor tissue.

DISCUSSION

The present study shows that ^{18}F-FDG uptake by VX2 liver tumors was 3.5-fold higher than that by normal liver tissue, and good contrast between the tumor and normal liver was achieved in PET scans.

Previous clinical studies have indicated that ^{18}F-FDG PET is a useful agent for positive imaging of liver tumors. For example, Yonekura et al. imaged three patients with

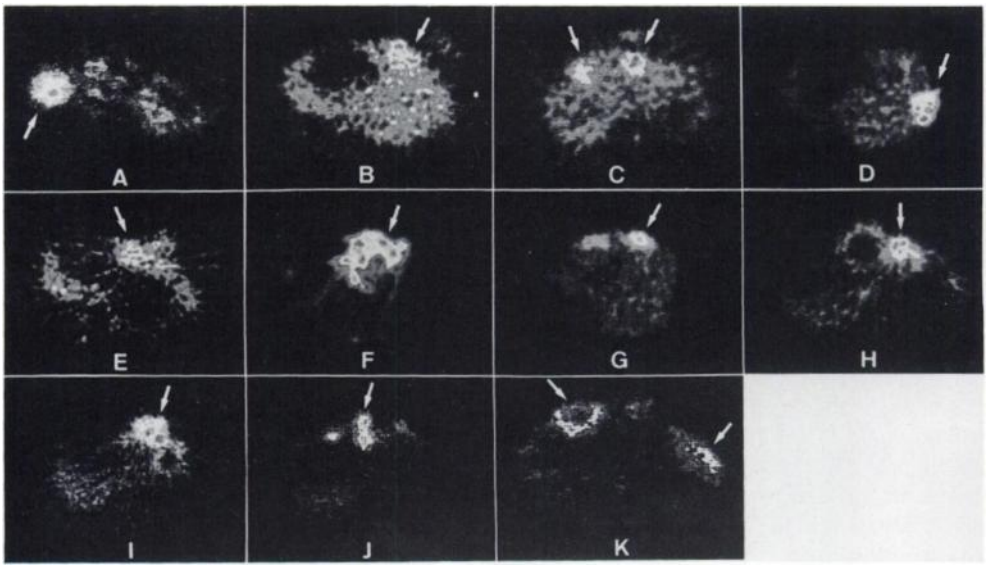

FIGURE 3. Fluorine-18-FDG PET images of VX2 liver tumors (arrows). A, B, C, D, E, F, G, H, I, J and K show the tumors in rabbits 5–15, respectively.

TABLE 1
Summary of the Values of Various Parameters in 15 Tumor-Bearing Rabbits

Rabbit no.	AI ((kBq/ml) × min)	C_l (kBq/ml)	C_l-to-AI (min^{-1})	C_t (kBq/ml)	C_t-to-AI (min^{-1})	C_t-to-C_l	$C_L(60)$ (kBq/ml)	$C_T(60)$ (kBq/ml)	K-complex (min^{-1})	Plasma glucose (g/dl)
1	4170	65.1	0.0156	215.6	0.0517	4.59				124
2	860	12.7	0.0148	39.8	0.0463	3.12				138
3	2530	27.3	0.0108	53.6	0.0212	1.96				126
4	720	9.6	0.0134	40.2	0.0558	4.16				123
5	1090	11.8	0.0108	44.7	0.0410	3.79	13.6	39.4	0.0322	175
6	1140	15.8	0.0139	58.5	0.0513	3.69	19.2	40.3	0.0294	
7	2030	25.0	0.0123	90.3	0.0445	3.61	23.7	68.7	0.0266	114
8	1110	21.3	0.0192	52.6	0.0474	2.47	13.7	41.5	0.0428	129
9	1060	11.7	0.0110	48.1	0.0454	4.12	13.7	46.0	0.0416	125
10	1880	17.3	0.0092	87.6	0.0466	5.05	21.9	73.7	0.0368	121
11	1520	21.1	0.0139	50.6	0.0333	2.40	18.7	69.0	0.0342	123
12	610						8.8	23.8	0.0394	241
13	2000						21.2	115.1	0.0589	111
14	1770						18.7	63.2	0.0340	113
15	760						9.8	26.3	0.0283	121
mean ± s.d.	1550 ± 890		0.0132 ± 0.0027		0.0440 ± 0.0091	3.54 ± 0.92			0.0367 ± 0.0086	135 ± 33

AI = arterial input; C_l = radioactivity in normal liver tissue excised 60 min after ^{18}F-FDG injection; C_t = radioactivity in tumor tissue excised 60 min after ^{18}F-FDG injection; $C_L(60)$ = radioactivity in normal liver tissue measured by PET 60 min after ^{18}F-FDG injection; $C_T(60)$ = radioactivity in tumor tissue measured by PET 60 min after ^{18}F-FDG injection.

liver metastases from colon carcinoma (*16*) and Messa et al. imaged four patients with liver metastasis from melanoma or breast cancer (*19*) using ^{18}F-FDG PET. Both studies suggested its usefulness for the detection and characterization of liver tumors. As reported by Nagata et al., ^{18}F-FDG PET is also a useful imaging modality for monitoring the response of liver tumors to treatment (*17*). Recently, Okazumi et al. reported on ^{18}F-FDG PET in 35 patients with liver tumors and demonstrated its usefulness for assessing the degree of differentiation of hepatocellular carcinoma as well as for making a differential diagnosis of liver tumors (*18*).

VX2 tumors implanted in rabbits have been widely used in various experimental studies, including evaluation of this tumor growing in the thigh muscle by using ^{18}F-FDG PET (*22*). VX2 can also be transplanted in the liver, as was done in the present study. Since this liver tumor model is of an adequate size to allow the performance of various types of experimental therapy, it is considered suitable for evaluation of the therapeutic response of liver tumors to different treatments. VX2 liver tumors can be evaluated by various imaging modalities. CT scanning and angiography show the morphological profile of the tumor, but the metabolic profile cannot be evaluated by these imaging methods. Histological examination and enzyme assays are useful for evaluating tumor metabolism, but the animal must be killed unless the tumor can be safely and accurately biopsied. Therefore, the establishment of a new method for evaluating tumor metabolism in vivo would be desirable. In the present study, the metabolic profile of VX2 tumors in rabbit livers was evaluated by ^{18}F-FDG PET, and our results suggest the utility of this method for the in vivo quantitative assessment of liver tumor metabolism.

TABLE 2
Activities of Key Carbohydrate-Metabolizing Enzymes in Tumor Tissue and Normal Liver Tissue

	Enzyme activity (mU/mg protein)*	
	VX2 liver tumor (n = 6)†	normal liver (n = 4)†
Hexokinase	4.2 ± 1.0	1.0 ± 0.2
Glucokinase	1.2 ± 0.2	1.7 ± 0.7
Phosphofructokinase	6.3 ± 4.6	5.5 ± 1.1
Pyruvate kinase	274.2 ± 110.4	21.3 ± 2.7
Glucose-6-phosphate dehydrogenase	5.2 ± 3.2	6.1 ± 1.4
Fructose-1,6-diphosphatase	0.9 ± 0.8	16.8 ± 2.3
Glucose-6-phosphatase	1.1 ± 0.8	41.1 ± 20.4

*Mean ± s.d.
†n = number of rabbits.

To determine whether the rabbit VX2 liver tumor model is appropriate for assessing the clinical usefulness of ^{18}F-FDG PET for liver, glucose metabolism of this tumor model must be compared with that of human liver tumors. Accordingly, we evaluated in vitro tumor tissue to normal liver tissue ^{18}F radioactivity ratio (C_t-to-C_l ratio), in vitro C_t-to-AI ratio and the in vivo K-complex value (determined as explained below).

Figure 4 summarizes the metabolic pathway of glucose. For quantitative measurement of ^{18}F-FDG accumulation in tumors, an appropriate compartment model is necessary. We applied the model shown in Figure 5, which is based on the following assumptions:

1. Fluorine-18-FDG-6-phosphate is not metabolized further, whereas glucose-6-phosphate enters the glycolytic pathway or the pentose phosphate pathway.
2. The membrane permeability of ^{18}F-FDG-6-phosphate is very low.
3. Dephosphorylation of ^{18}F-FDG-6-phosphate is negligible in the tumors, because of its low glucose-6-phosphatase activity.

On the basis of this model, we used a graphical method to determine the tumor accumulation of ^{18}F-FDG, which was regarded as equivalent to the K-complex, i.e., $(k_1 \times k_3)/(k_2 + k_3)$, where k_1, k_2 and k_3 are respectively the rate of glucose inflow, glucose outflow and phosphorylation.

When X and Y are defined as follows:

$$X = \frac{\int_0^t C_P(\tau)\, d\tau}{C_P(t)},$$

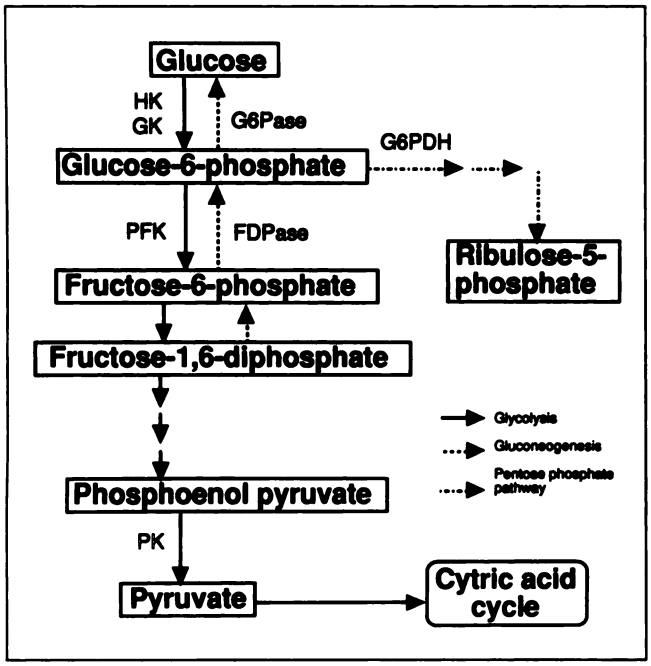

FIGURE 4. Summary of the metabolic pathway of glucose.

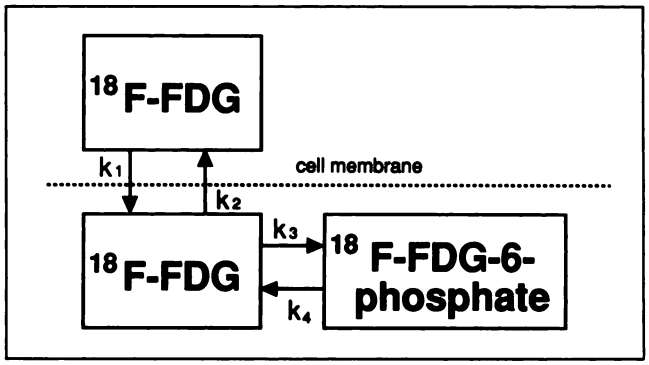

FIGURE 5. Compartment model used for assessing ^{18}F-FDG handling by VX2 tumor cells. k_1, k_2, k_3 and k_4 are rate constants.

$$Y = \frac{C_T(t)}{C_P(t)},$$

the curve produced by plotting Y versus X becomes a straight line with slope K, and the K-complex is determined as the slope of this line (*31,32*). Table 1 summarizes data on the C_t-to-C_l ratio, C_t-to-AI ratio and K-complex for the 15 tumor-bearing rabbits.

In previous studies on human liver tumors, the tumor-to-normal liver tissue ratio was 3.3–4.7 for liver metastases from colon carcinoma (*16*), while the K-complex value was 0.0358 min^{-1} for liver metastases from melanoma (*19*) and was 0.0304 min^{-1} for liver metastases from colon, esophageal, gastric, and pancreatic cancer (*18*). In this study, as shown in Table 1, the tumor-to-normal liver tissue ratio and the K-complex value of VX2 liver tumors were respectively 3.5 ± 0.9 and 0.037 ± 0.009 min^{-1} (n = 11). This correlates well with the clinical data. Thus, this tumor model seems to be comparable with human liver tumors. However, human tumors could have considerable variability in their metabolic profiles, while only one type of tumor was examined in this study. Therefore, the inferences derived from this model should be limited to tumors in which k_3 is relatively high and k_4 (the rate of dephosphorylation) is nearly zero, such as metastatic liver tumors.

The enzyme activity study revealed that transplanted VX2 liver tumors had increased HK and PK activity with decreased G6Pase and FDPase activity, when compared with normal liver tissue. It is possible that the enzyme activity might have been altered because tissue excision was performed under general anesthesia and the samples were frozen after excision. Despite these potential limitations of the experimental method, the data on enzyme activities corresponded well with accelerated glycolytic rate of the tumor and the comparative dephosphorylation in normal liver tissue. However, this enzymatic profile could not completely account for the accumulation of ^{18}F-FDG in transplanted VX2 liver tumors or for the low background radioactivity of the surrounding liver, probably because both the K-complex value and the tumor-to-normal liver tissue ratio of ^{18}F-FDG uptake depend not only on k_3 and k_4 (i.e., phosphorylation and dephosphorylation) but

also on k_1 and k_2 (i.e., the forward and reverse ^{18}F-FDG transfer rates). Despite this, the enzyme activity data supported the quality of the tumor images obtained with ^{18}F-FDG PET.

We therefore conclude that this transplanted VX2 liver tumor model with ^{18}F-FDG PET evaluation is useful for the following reasons:

1. Fluorine-18-FDG PET can detect changes in tumor metabolism which may precede morphological changes.
2. Fluorine-18-FDG PET can be performed in vivo, and therefore the changes during and after treatment can be evaluated.
3. The images obtained are clear enough for quantitative assessment.
4. The C_t-to-C_1 ratio and K-complex values of the model corresponded approximately to those reported for human liver tumors.
5. The activity profile of the key carbohydrate-metabolizing enzymes in this liver tumor model agreed with tumor handling of ^{18}F-FDG.

Another advantage of this model is that experimental therapies such as transcatheter arterial embolization (*33*), hyperthermia or irradiation can be performed easily. In the future, this model may be applied for in vivo evaluation of various therapeutic modalities.

ACKNOWLEDGMENTS

The authors thank Hamamatsu Photonics K. K. for developing and supplying the animal PET system.

REFERENCES

1. Burk D, Wood M, Hunter J. On the significance of glycolysis for cancer growth with special references to Moris rat hepatomas. *J Natl Cancer Inst* 1967;38:839–863.
2. Sweeney MJ, Ashmore J, Morris HP, Weber G. Comparative biochemistry of hepatomas. IV. Isotope studies of glucose and fructose metabolism in liver tumors of different growth rates. *Cancer Res* 1963;23:995–1002.
3. Lo C, Cristofalo VJ, Morris HP, Weinhouse S. Studies on respiration and glycolysis in transplanted hepatic tumors of the rat. *Cancer Res* 1968;28:1–10.
4. Som P, Atkins HL, Bandoypadhyay D, et al. A fluorinated glucose analog, 2-fluoro-2-deoxy-D-glucose (^{18}F): nontoxic tracer for rapid tumor detection. *J Nucl Med* 1980;21:670–675.
5. Phelps ME, Huang S-C, Hoffman EJ, Selin C, Sokoloff L, Kuhl DE. Tomographic measurement of local cerebral glucose metabolic rate in humans with (F-18)-2-fluoro-2-deoxy-D-glucose: validation of method. *Ann Neurol* 1979;6:371–388.
6. Hawkins RA, Phelps ME, Huang S-C. Effects of temporal sampling, glucose metabolic rates and disruptions of the blood-brain barrier on the FDG model with and without a vascular compartment: studies in human brain tumors with PET. *J Cereb Blood Flow Metab* 1986;6:170–183.
7. Di Chiro G. Positron emission tomography using [^{18}F] fluorodeoxyglucose in brain tumors: a powerful diagnostic and prognostic tool. *Invest Radiol* 1987;22:360–371.
8. Kubota K, Matsuzawa T, Fujiwara T, et al. Differential diagnosis of lung tumor with positron emission tomography: a prospective study. *J Nucl Med* 1990;31:1927–1932.
9. Abe Y, Matsuzawa T, Fujiwara T, et al. Clinical assessment of therapeutic effects on cancer using ^{18}F-2-fluoro-2-deoxy-D-glucose and positron emission tomography: preliminary study of lung cancer. *Int J Radiat Oncol Biol Phys* 1990;19:1005–1010.
10. Haberkorn U, Strauss LG, Dimitrakopoulou A, et al. PET studies of fluorodeoxyglucose metabolism in patients with recurrent colorectal tumors receiving radiotherapy. *J Nucl Med* 1991;32:1485–1490.
11. Strauss LG, Clorius JH, Schlag P, et al. Recurrence of colorectal tumors: PET evaluation. *Radiology* 1989;170:329–332.
12. Minn H, Paul R, Ahonen A. Evaluation of treatment response to radiotherapy in head and neck cancer with florine-18-fluorodeoxyglucose. *J Nucl Med* 1988;29:1521–1525.
13. Haberkorn U, Strauss LG, Reisser Ch, et al. Glucose uptake, perfusion and cell proliferation in head and neck tumors: relation of positron emission tomography to flow cytometry. *J Nucl Med* 1991;32:1548–1555.
14. Hawkins RA, Hoh C, Dahlborn M, et al. PET cancer evaluations with FDG. *J Nucl Med* 1991;32:1555–1558.
15. Hawkins RA, Choi Y, Huang S-C, Messa C, Hoh CK, Phelps ME. Quantitating tumor glucose metabolism with FDG and PET. *J Nucl Med* 1992; 33:339–344.
16. Yonekura Y, Benua RS, Brill AB, et al. Increased accumulation of 2-deoxy-2-^{18}F-fluoro-D-glucose in liver metastases from colon carcinoma. *J Nucl Med* 1982;23:1133–1137.
17. Nagata Y, Yamamoto K, Hiraoka M, et al. Monitoring liver tumor therapy with ^{18}F-FDG positron emission tomography. *J Comput Assist Tomogr* 1990;14:370–374.
18. Okazumi S, Isono K, Enomoto K, et al. Evaluation of liver tumors using fluorine-18-fluorodeoxyglucose PET: characterization of tumor and assessment of effect of treatment. *J Nucl Med* 1992;33:333–339.
19. Messa C, Choi Y, Hoh CK, et al. Quantification of glucose utilization in liver metastases: parametric imaging of FDG uptake with PET. *J Comput Assist Tomogr* 1992;16:684–689.
20. Abe Y, Matsuzawa T, Fukuda H, et al. Experimental study for tumor detection using ^{18}F-2-fluoro-2-deoxy-D-glucose: imaging of rabbit VX2 tumor with single photon gamma gamera. *Kaku Igaku* 1985;22:389–391.
21. Abe Y, Matsuzawa T, Fujiwara T, et al. Assessment of radiotherapeutic effects on experimental tumors using ^{18}F-2-fluoro-2-deoxy-D-glucose. *Eur J Nucl Med* 1986;12:325–328.
22. Fukuda H, Matsuzawa T, Abe Y, et al. Experimental study for cancer diagnosis with positron-labeled fluorinated glucose analogs. Fluorine-18-2-fluoro-2-deoxy-D-mannose: a new tracer for cancer detection. *Eur J Nucl Med* 1982;7:294–297.
23. Fukuda H, Toshioka S, Watanuki S, et al. Experimental study for cancer diagnosis with ^{18}FDG: differential diagnosis of inflammation from malignant tumor. *Kaku Igaku* 1983;20:1189–1192.
24. Iosilevski G, Front D, Bettman L, Hardoff R, Ben-Arieh Y. Uptake of gallium-67-citrate and [2-^{3}H] deoxyglucose in the tumor model, following chemotherapy and radiotherapy. *J Nucl Med* 1985;26:278–282.
25. Kubota K, Ishiwata K, Kubota R, et al. Tracer feasibility for monitoring radiotherapy: a quadruple tracer study with florine-18-fluorodeoxyglucose or fluorine-18-fluorodeoxyuridine, L-[methyl-^{14}C] methionine, [6-^{3}H] thymidine and gallium-67. *J Nucl Med* 1991;32:2118–2123.
26. Shiue C-Y, Salvadori PA, Wolf AP, Fowler JS, MacGregor RR. A new improved synthesis of 2-deoxy-2-[^{18}F]fluoro-D-glucose from ^{18}F-labeled acetyl hypofluorite. *J Nucl Med* 1982;23:899–903.
27. Watanabe M, Uchida H, Okada H, et al. A high resolution PET for animal studies. *IEEE Trans Med Imaging* 1992;11:577–580.
28. Taketa K, Tanaka A, Watanabe A, Takesue A, Aoe H, Kosaka K. Undifferentiated patterns of key carbohydrate-metabolizing enzymes in injured livers. I. Acute carbon-tetrachloride intoxication of rat. *Enzyme* 1976;21: 158–173.
29. Taketa K, Shimamura J, Takesue A, Tanaka A, Kosaka K. Undifferentiated patterns of key carbohydrate-metabolizing enzymes in injured livers. II. Human viral hepatitis and cirrhosis of the liver. *Enzyme* 1976;21:200–210.
30. Taketa K, Shimamura J, Ueda M, Shimada Y, Kosaka K. Profiles of carbohydrate-metabolizing enzymes in human hepatocellular carcinomas and preneoplastic livers. *Cancer Res* 1988;48:467–474.
31. Patlak CS, Blasberg RG, Fenstermacher JD. Graphical evaluation of blood-to-brain transfer constants from multiple-time uptake data. *J Cereb Blood Flow Metab* 1983;3:1–7.
32. Patlak CS, Blasberg RG. Graphical evaluation of blood-to-brain transfer constants from multiple-time uptake data. Generalizations. *J Cereb Blood Flow Metab* 1985;5:584–590.
33. Hase M, Sako M, Hirota S. Experimental study of ferromagnetic induction heating combined with hepatic arterial embolization for treatment of liver tumors. *Nippon Act Radiol* 1990;50:1402–1414.